Thermal Conductivity of Oriented Single Crystals of
Hexagonal Close-Packed Helium 4[†]

E. M. Hogan,[*] R. A. Guyer,[‡] and H. A. Fairbank

Department of Physics, Duke University, Durham, North Carolina 27706

(Received 17 May, 1968; revised manuscript received 14 February 1969)

Thermal conductivity measurements have been made on hcp single crystals of helium 4 between 0.36°K and 1.6°K. Data on crystals grown at 53.4, 85, and 125.8 atm exhibit a strong orientation dependence in the umklapp region, and Poiseuille flow at temperatures below the thermal conductivity maximum. In the umklapp region, the data are described by two thermal conductivities, $K_\perp = A_\perp \exp(\Theta_D/2.58T)$ and $K_\parallel = A_\parallel \exp(\Theta_D/4.62T)$, the components of the thermal conductivity tensor perpendicular and parallel to the c axis. At 85 atm, $A_\perp = 1.12 \times 10^{-5}$ W/cm °K and $A_\parallel = 2.31 \times 10^{-4}$ W/cm °K. The umklapp data permit one to determine the orientation of the single crystals. The thermal conductivity in the Poiseuille region is proportional to $d^2 T^6$, where d is the sample diameter. The normal-process relaxation time determined from these data, $\tau_N = (2.1 \pm 0.4) (\Theta_D/T)^3 \times 10^{-12}$ sec, is in good agreement with the results of second-sound experiments.

I. INTRODUCTION

Solid helium crystals have proved to be a particularly suitable laboratory for testing phonon-gas transport phenomena. Solid He[3] and He[4] samples can be made with extraordinary chemical and isotopic purity over a wide range of density and pressure. Thermal conductivity data have been taken from below 1°K to the melting temperature from 25 to about 2000 atm.[1] Until recently, all measurements were made on samples grown at constant volume by the blocked capillary method.[1] Such samples are probably polycrystalline and not defect free. Measurements on polycrystalline samples do not exhibit Poiseuille flow[2] or anisotropy effects.[3] Good single crystals of solid helium can be grown by the constant pressure technique developed by Shal'nikov[4] and Mezhov-Deglin.[5] Mezhov-Deglin has made a series of thermal conductivity measurements[5-7] on single crystals of hcp He[4] grown at four pressures: 60, 85, 153, and 185 atm. He has observed Poiseuille flow and verified the d^2 dependence of thermal conductivity on sample diameter for this phenomenon; he has also observed anisotropy in the thermal conductivity at temperatures above the low-temperature maximum.

In this paper we report the results of an investigation of the thermal conductivity in single crystals of hcp He[4] grown at constant pressures of 53, 85, and 126 atm.[8] These measurements are more extensive and, we believe, more accurate than the earlier results of Mezhov-Deglin. They admit to a simple analysis by which the microscopic scattering rates can be determined. It is possible from the analysis of the data in the high-temperature umklapp region to determine λ_U^Z (the umklapp[9] mean free path in the Ziman limit[2]) and the angular orientation of the samples.[3] The analysis of the data just below the low-temperature maximum yields λ_N (the normal process[9] mean free path).

In Sec. II we review the relevant theoretical results which we will use in discussing the conditions to be met in doing the experiment and in analyzing the results. In Sec. III we discuss the apparatus and experimental procedures. In Sec. IV we discuss the data and its analysis.

II. BACKGROUND

At low temperatures the phonon gas in a dielectric solid can be described by a set of macroscopic equations derived by Guyer and Krumhansl.[2, 10] They discuss in detail the solution to these equations and the implication of the solution for thermal conductivity measurements. The result of that discussion which is relevant to the present experiment is that at low temperatures, there are three temperature regions in which the thermal conductivity K has qualitatively different behavior: the boundary region, the Poiseuille region, and the Ziman region. We review the behavior of K in each of these regions.

(1) *The boundary region.* This region occurs at lowest temperatures when $\lambda_N \gg d$ and $\lambda_R^Z \gg d$; λ_N is the N-process mean free path, λ_R^Z is the resistive process mean free path computed in the Ziman limit, and d is the sample chamber diameter. The thermal conductivity in this region is given by

$$K_b = \tfrac{1}{3} C_v c \alpha d , \qquad (1)$$

where C_v is the specific heat per unit volume, c is the Debye velocity of sound, and α is a constant on the order of 1. Measurement of K in this region provides a measure of crystal quality.

(2) *The Poiseuille region.* This region occurs just below the low-temperature maximum when one of the inequalities reverses, $\lambda_N \ll d$ and $\lambda_R{}^Z \gg d^2/\lambda_N$. The thermal conductivity in this region is given by

$$K_P = \tfrac{1}{3} C_v \tfrac{5}{32} d^2/\tau_N , \qquad (2)$$

and provides a direct measure of τ_N, the normal-process relaxation time. In this region the thermal conductivity mean free path is greater than d by the factor $\tfrac{5}{32}(d/\lambda_N)$.

(3) *The umklapp region (Ziman limit).* This region occurs just above the low-temperature maximum when $\lambda_N \ll \lambda_R$ and $\lambda_R \ll d$, where λ_R is the mean free path due to all resistive scattering processes. The thermal conductivity in this region is given by

$$K_Z = \tfrac{1}{3} C_v c\lambda_R{}^Z , \qquad (3)$$

where $\lambda_R{}^Z$ is the resistive process mean free path computed in the Ziman limit. In this experiment since the only resistive scattering mechanism is umklapp scattering, we have $\lambda_R{}^Z = \lambda_U{}^Z$.

As the temperature is increased further above the Ziman region, the limit $\lambda_N \ll \lambda_R{}^Z$ which obtains in the Ziman region breaks down. The thermal conductivity is given by Eq. (3) with $\lambda_R{}^Z$ replaced by $\lambda_R{}^K$, the resistive mean free path computed in the kinetic limit. The data presented in this paper do not go to sufficiently high temperature to reach the kinetic region.

The solution to the coupled macroscopic equations[2] in the region of $T_{\max}$ is

$$K = \tfrac{1}{3} C_v c\lambda_R{}^Z G(\mu), \qquad (4)$$

where $G(\mu) = 1 - \dfrac{2 J_1(id/2\beta)}{(id/2\beta) J_0(id/2\beta)}$,

$\mu = d^2/\beta^2$, and $\beta^2 = \lambda_N \lambda_R{}^Z/5$. Above $T_{\max}$, $\mu \gg 1$ and $G(\mu) \sim 1$, and Eq. (4) goes over to Eq. (3). Below $T_{\max}$, $\mu \ll 1$ and $G(\mu) \sim \mu/2$, and Eq. (4) goes over to Eq. (2). It is *only* in the region of $T_{\max}$ that a single analytic expression for K exists which depends sensitively on all of the scattering rates characterizing the phonon gas.

The thermal conductivity of hcp helium crystals at temperatures above $T_{\max}$ exhibits a very large temperature-dependent anisotropy which has already been reported.[3] Anisotropy in K can arise from two causes, anisotropy in the velocity of sound and anisotropy in the phonon scattering rate.

In the usual derivation of an equation for K, e.g., Eq. (3), it is assumed that c and the scattering rate are isotropic. If these conditions are relaxed, the most general relation which can be written relating the heat current density $\vec{Q}$ and the temperature gradient $\vec{\nabla} T$ is

$$Q_\beta = -\sum_\gamma C_v(T) c_\beta (R^{-1})_{\beta\gamma} c_\gamma \nabla_\gamma T , \qquad (5)$$

where $R(q)$ is the umklapp scattering rate; $(R^{-1})_{\beta\gamma}$ is the $\beta, \gamma\, q$ – space matrix element of R.[2] It is weighted in the direction of the heat current flow by a factor $\cos^2\theta$. If R is isotropic, then any anisotropy of K is due to anisotropy in the velocity of sound. Equation (5) admits the possibility in principle of anisotropy in K.

There is a further strong condition imposed on K by crystal symmetry. K is a tensor of rank two which relates $\vec{Q}$ and $\vec{\nabla} T$, and therefore, it must obey the requirements imposed by the symmetry of the crystal structure on such tensors. For a cubic crystal, K has three equal diagonal components; there is no anisotropy. For a hcp crystal K has the form[11]

$$\overleftrightarrow{K} = \begin{pmatrix} K_\perp & 0 & 0 \\ 0 & K_\perp & 0 \\ 0 & 0 & K_\parallel \end{pmatrix}, \qquad (6)$$

where the z axis is along the c axis of the crystal and the x-y plane is perpendicular to the c axis. If θ is the angle between the direction of the heat current and the c axis of the crystal, the thermal conductivity in the direction of $\vec{Q}$ is given by

$$\frac{1}{K(T, \theta)} = \frac{1}{K_\parallel(T)} \cos^2\theta + \frac{1}{K_\perp(T)} \sin^2\theta . \qquad (7)$$

For a polycrystalline sample, the thermal conductivity is given by an angular average of Eq. (7),

$$\overline{K} = 3K_\parallel(T) K_\perp(T)/[2K_\parallel(T) + K_\perp(T)] . \qquad (8)$$

The thermal conductivity should be given by Eq. (7) at temperatures where K can be regarded as a bulk property of the solid, i.e., the umklapp region. In both the Poiseuille and boundary regions, K is limited by the geometry of the sample, and Eq. (7) does not apply.

In the boundary region, the heat current is carried by the phonons traveling along the axis of the sample. The thermal conductivity in the boundary region depends upon the phonon velocity c_a along the axis in the form[12]

$$K = \tfrac{1}{3} C_v cd(c/c_a)^2 . \qquad (9)$$

III. EXPERIMENTAL

The apparatus used for growing the crystals and measuring their thermal conductivities is shown in Fig. 1. The He^4 pot had a volume of 250 cm^3, and was filled from the bath of He^4 surrounding the exchange gas can by means of a needle valve connecting the bath with the manometer line to the He^4 pot. The pot could be pumped to a temperature of about 1.0°K and operate for 36 h or more between fillings. In taking data, a crystal was grown and all data were taken between two fillings to avoid subjecting the crystal to the rapid temperature changes associated with filling the He^4 pot. The He^3 pot had a volume of 6.7 cm^3 and was machined from a single piece of electrolytic copper, including the $\frac{1}{8}$-in.-thick plate on which the
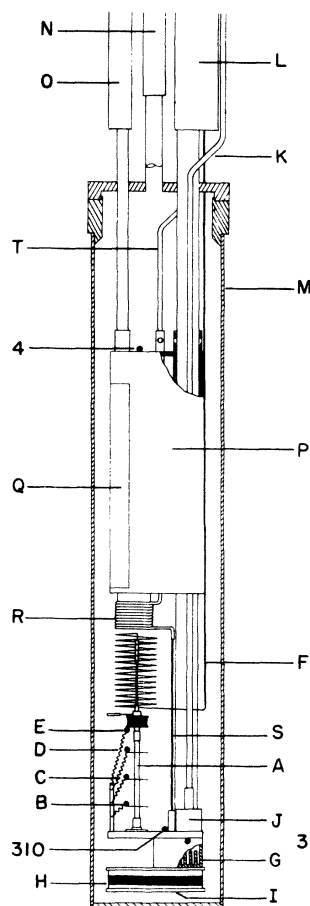
FIG. 1. Experimental arrangement. M is the exchange gas can, P is the He^4 pot, and G is the He^3 pot. H and Q are the pot heaters. A is the sample chamber, and F is the filling capillary. B, C, D, E, 3, 4, and 310 are the resistance thermometers, and J is the He^3 manometer pot. L is the He^3 pumping line, and R is the He^3 recondensation line.

sample chambers were mounted. Fins on the bottom of the He^3 pot reduced the Kapitza temperature difference between the He^3 and the copper at high-heat inputs. The small (17-cm^3) He^4 pot attached to the He^3 pot was used for growing crystals, and will be referred to as the "$He^{4\prime}$ pot" in this paper to distinguish it from the large He^4 pot. Both pots are equipped with heaters and with germanium resistance thermometers R_3 and R_4. The carbon resistance thermometer R_{310} was used at the lowest temperatures. The separate manometer pot, filled with He^3 and connected to oil and mercury manometers, is hard soldered to the plate forming the top of the He^3 pot, and serves as the primary vapor-pressure thermometer. This He^3 manometer system could be used up to 2.5°K with the amount of pure He^3 available, above which temperature the germanium thermometers were calibrated in the He^4 bath. The He^3 system was provided with a continuous recondensation capability, but this was never used during calibration or data taking, as it tended to cause fluctuations in temperature while taking points.

The sample chamber was filled with helium by a length of 0.025-in.-o.d. ×0.014-in.-i.d. cupronickel capillary extending from the Dewar head to a point just above the He^4 pot, where it is soft soldered onto a piece of 0.014-in.-o.d. ×0.006-in.-i.d. cupronickel capillary which was soldered to the He^4 pot with Wood's metal and then formed into a free-standing coil, which was connected to the sample chamber itself. To prevent possible apparatus vibrations from flexing the coil, a brace was made by slotting one end of a piece of 0.083-in.-o.d. stainless-steel tubing and gluing the 0.014-in.-o.d. tubing into this slot at the point where it first becomes horizontal after leaving the He^4 pot. The other end of this brace was soldered to the He^4 pot with Wood's metal, and the length of free capillary between the brace and the sample chamber was 42 in.

The sample chamber proper is shown in Fig. 2. The fill capillary is soft soldered into the copper sleeve at the top of the chamber, and the auxiliary tube at the side is capped off after air is blown through the main capillary to check for possible plugged joints resulting from the assembly process. The top of the sample chamber is turned from electrolytic copper, and is provided with a heater of No. 40 Manganin wire, with a resistance of 2000 Ω. The sample chamber is made of stainless-steel tubing, 0.177-cm i.d. ×0.242-cm o.d. in the small chamber and 0.268-cm i.d. ×0.321-cm o.d. in the large chamber. The three fins along the chamber wall are 0.010 in. thick and are hard soldered to the chamber. The bottom of the sample chamber is made of electrolytic copper, and is soldered with Wood's metal to the plate forming the top of the He^3 pot. The thermometers, marked B, C, D, E, and 310, are $\frac{1}{10}$-W
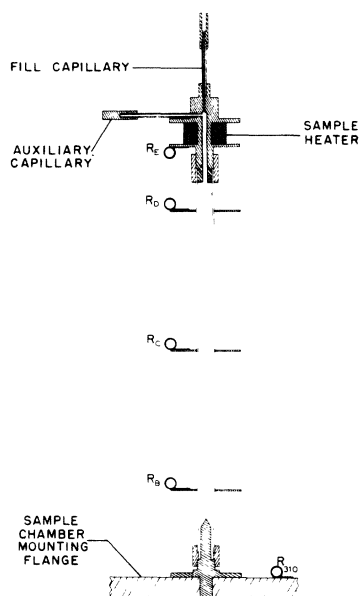
FIG. 2. Sample chamber. B, C, D, E, and 310 are the resistance thermometers, and the mounting flange is on the He^3 pot.

Allen-Bradley resistors cemented with Epoxy resin into three turns of 0.005-in. copper foil soldered together and fastened to the fins with Wood's metal. All connections to the resistors and to the sample heater are thermally anchored to the He^3 pot, but this is not possible for the fill capillary due to the crystal growing process employed. The effects of this arrangement will be discussed later in this section.

The thermometers are calibrated against the vapor pressure of He^3 given by the T_{62} temperature scale with corrections for the thermomolecular effect.[13] The heat input Q is measured by a four-wire potentiometric technique. The data are analyzed by a computer program using logic similar to that of Bertman *et al.*

In growing a crystal, the shape of the pin in the bottom of the sample chamber is such that growth of crystals nucleated on it should be substantially normal to the copper-helium interface until the crystals encounter the sample chamber wall, since the conductivity of the copper at the growing temperature is 10^3 times that of the liquid helium or of the stainless steel. Thus the crystal nucleated at the tip of the pin should (in principle, at least) grow out to the sample chamber walls before any competing crystal can get past it, and seal off any competing crystals in a region below the first thermometer fin. The large area of helium-copper interface created by the sides of the pin also serve to reduce the Kapitza temperature difference between the crystal and the copper, which

can be as high as 0.2°K for some of the data.

To grow a crystal, He^4 is first condensed into the He$^{4'}$ pot and the entire system is brought to 4.2°K. The fill capillary is tested for blockage by suddenly lowering the pressure in the high-pressure system and watching resistors R$_3$ and R$_E$ cool as the material in the sample chamber cools adiabatically. The proper growth pressure is then set, and the system is allowed to come to thermal equilibrium at 4.2°K. The He^4 pot is then closed off from the bath, pumped to 0.2°K above the melting point of the helium sample and regulated. Once the system has come into equilibrium at this new temperature, a miniature needle valve connecting the He$^{4'}$ pot to a vacuum pump is opened by a predetermined amount and enough power is put into the sample heater to maintain a temperature difference of about 0.2°K across the liquid-filled sample chamber. While the cooling proceeds, the resistors 3, B, C, D, and E are monitored sequentially. The passage of the liquid-solid interface is signalled by a slowing and subsequent speeding up of the rate of cooling of a given resistor, due to the evolution of the latent heat of fusion at the interface. Once the resistors are calibrated, the passage of the interface is more simply noted by the passage of the resistors through the appropriate resistance values. When the crystal is complete, the evolution of latent heat is reduced because of the smaller area of the fill capillary, and the top of the crystal cools rapidly. At this point the power into the sample heater is reduced linearly with time by a circuit due to Crooks,[14] while the He$^{4'}$ pot is now pumped more rapidly until its temperature is at the λ point. The temperature of the He^4 pot is now brought to just above the λ point and regulated, while the He$^{4'}$ pot valve is gradually opened to maximum. When the thermocouple gauge on the He$^{4'}$-pot pumping line reads less than 20-mTorr pressure the pot is closed off, the He^4 pot is cooled to 1.6°K, and data are taken.

As mentioned earlier, the geometry of the sample chamber bottom is supposed to yield a single unstressed crystal in the measuring region of the sample chamber, and some good crystals have been obtained in this way without any other processing. (An example of such a crystal is that in Run 11-1.) In general, however, the highest conductivities below T_{max} were obtained when the He$^{4'}$ pot was shut off during the growth process, and the temperature of the He^3 pot raised and regulated in such a way that the interface was stopped just above R$_B$ for annealing. We annealed for three hours for convenience, but there is nothing to indicate that this time could not be shorter. Annealing with the interface anywhere within the sample chamber (but not within the fill capillary) gave good crystals most of the time, but the position just above R$_B$

seemed to be the most reliable. This may be due to the removal of defects created by the rapid freezing of the material around the nucleation post.

Several constant volume crystals were also grown during the experiment by bringing both pots into thermal equilibrium at $0.05°K$ above the liquidus temperature and then cooling the He^4 pot as rapidly as possible to block the fill capillary with solid He^4 before freezing the main sample. No attempts at annealing these crystals were made, as polycrystalline specimens were desired for use in assigning orientations to the constant pressure crystals through the use of Eq. (8). Very low boundary conductivities were obtained for these crystals, which suggests that the specimens were indeed highly polycrystalline.

Once the crystal reached $1.6°K$, data were taken by the method of Bertman et al., [15] with modifications necessitated by the placement of our filling capillary. In the region above $1.0°K$, heat was fed into the sample heater sufficient to maintain a temperature difference of $0.1°K$ between the He^3 pot and the top of the sample chamber. Both temperatures were monitored while the power level was being set. The temperature of the He^4 "pot" was made equal to that of resistor E to avoid possible errors due to heat leaks down the filling capillary, which was the only connection to the sample chamber which was not heat-sinked to the He^3 pot. In the region below $1°K$, the He^4 pot was allowed to pump at full speed, which maintained a temperature of $1.0°K$. As the peak conductivities were approached, the temperature differences between adjacent fins were reduced from their high-temperature values by Kapitza boundary resistances, reaching minimum values of about 1 m$°K$ for the data at the peak of the curve. Data were taken down to about $0.36°K$, where the resistors used went over 1.1 MΩ. The error signal from the He^3-pot thermometry bridge was used to provide automatic temperature regulation of the He^3 pot during measurements, freeing the operator to take the data with a second bridge.

The heat leak down the fill capillary into the sample chamber can create experimental error leading to apparent conductivities higher than the true values at the lowest temperatures. This effect was corrected for in the data presented in this paper by calibrating the thermometer resistors on each crystal immediately after taking the thermal conductivity data. The temperature of the He^4 pot was also regulated to assure that its temperature remained the same for datum points and for calibration points.

Our thermometry was done via ac Wheatstone bridges with lock-in signal detection such that power into the measuring resistors was never more than 10^{-12} W. The bridges were sensitive

to a $\Delta R/R$ of one part in 10^4. Calibration points of R_B against He^3 vapor pressure gave a fit with an rms deviation of less than 10^{-3} $°K$, with the largest contribution at low-vapor pressures as expected. All measuring resistors were fitted to the vapor pressure calibration points as a check for possible errors in transcribing calibration data, and these fits were found to agree with each other to better than 10^{-4} $°K$. Sample chambers were carefully measured, and the L/A term in the conductivity is accurate to $\pm 0.7\%$. The heat input Q is known to $\pm 0.1\%$. With these figures and the consistency of the data, we feel that the thermal conductivity results given in this paper may be taken as being accurate to better than $\pm 2\%$ in all ranges. Relative values of thermal conductivity points within a given run should be accurate to within $\pm 1\%$.

IV. RESULTS AND DISCUSSION
A. Umklapp Region

Measurements of the thermal conductivity were made in single crystals of hcp He^4 grown in the manner described above at constant pressures of 53.4, 85, and 125.8 atm. Representative results on good single crystals are presented in the Appendix. The most extensive data are at 85 atm, a pressure we chose because it is also the pressure at which Mezhov-Deglin's data are most complete. The discussion in this section will be primarily about our 85 atm data. Where it is illuminating to consider the results obtained at other pressures, we do so.

27 crystals were grown at a constant pressure of 85 atm. Of these, ten were grown in a sample chamber of diameter $d = 1.77$ mm, and 17 were grown in a sample chamber of diameter $d = 2.68$ mm. Of the 27 crystals grown at 85 atm, 21 were not "split" in the umklapp region.[3] As used in this paper, a crystal is "split" at some temperature T if the K values of the upper and lower halves of the specimen differ by more than 10%. In Fig. 3 we show the data on four representative crystals grown in the 2.68-mm-diam sample chamber. The basic feature of this data which we want to emphasize in the early part of this discussion is the wide range of variation in K at fixed T above T_{max}. As has been pointed out, this variation is evidence for a strong *scattering* anisotropy in the umklapp region.[3] It is possible to use this anisotropy to determine the orientation of the crystals in the sample chamber.

Of the 21 "unsplit" crystals which we regard as giving good umklapp data, the highest umklapp thermal conductivity was observed in crystal 11-12, the closed triangles in Fig. 3. This crystal had an umklapp conductivity about equal to that of MD-I which at the time of the previous pub-
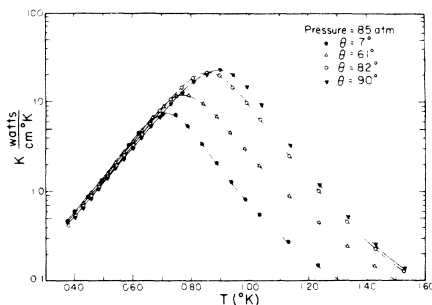
FIG. 3. Typical thermal conductivity results at 85 atm. Data from these crystals are presented in the Appendix.

lication[3] had the highest 85-atm umklapp conductivity measured. The lowest umklapp thermal conductivities were obtained in crystal 10-10. These data may be inserted into Eq. (8) to yield a prediction of the thermal conductivity $\bar{K}$ of a randomly oriented polycrystal for each of the two possible assignments of $K_\perp$ and $K_\parallel$ to crystals 11-12 and 10-10. These predictions have been plotted in Fig. 4. Comparison of the two predictions with the polycrystalline data of crystal 10-2 leads to the identification of the highest K with $K_\perp$ in Eq. (6) and the lowest K with $K_\parallel$ in Eq. (6). The thermal conductivity perpendicular to the c axis of the crystal is that of crystal 11-12, and can be represented analytically by

$$K_\perp(T) = 1.12 \times 10^{-5} e^{14.2°K/T} \text{ W/cm °K.} \quad (10)$$

Similarly, the thermal conductivity parallel to the c axis of the crystal is that of crystal 10-10. Thus $K_\parallel(T)$ is given by

$$K_\parallel(T) = 2.31 \times 10^{-4} e^{7.94°K/T} \text{ W/cm °K.} \quad (11)$$

These limits are plotted as solid lines in Fig. 5 along with typical 85-atm umklapp data from both sample chambers. It should be possible to construct the umklapp K of any crystal lying between 11-12 and 10-10 by taking the linear combination given by Eq. (7) for a single θ at each T in the umklapp region. We find that a unique θ can be associated with each crystal which gives $K(T)$ from Eqs. (7), (10), and (11) exactly. Thus it is possible to determine the angular orientation of the crystals in the sample chamber. The crystals shown in Fig. 3, for example, are at 7°, 61°, 82°, and 90°. The solid curves drawn through the data in Fig. 5 are constructed from Eq. (7) using these angles. Angles were obtained from the umklapp data for each crystal and will be used to label crystals in subsequent discussion.

The method used to determine θ assumes that the measurements cover the full range of possible crystal orientations. The fact that only the limiting conductivity curves of Fig. 5 are good straight lines in the umklapp region, as pre-
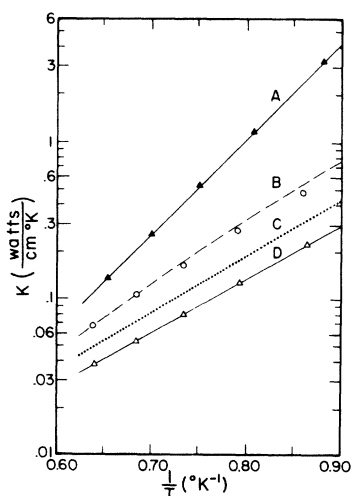
FIG. 4. Choosing $K_\perp$ and $K_\parallel$. The closed triangles are data from Run 11-12; the open triangles from Run 10-10. The dashed line represents the prediction of Eq. (8) for $\bar{K}$ if Run 11-12=$K_\perp$ and Run 10-10=$K_\parallel$; the dotted line is the same prediction if Run 11-12=$K_\parallel$ and Run 10-10=$K_\perp$. The open circles are data from a typical polycrystal, Run 10-2.
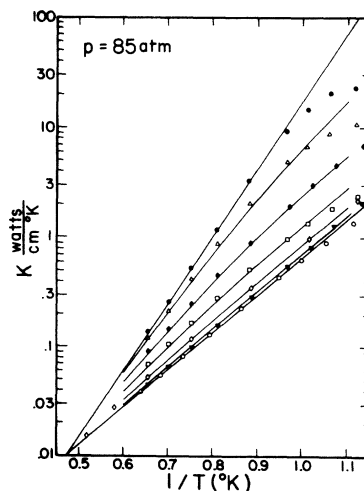
FIG. 5. Typical umklapp data at 85 atm. The upper and lower limiting lines represent $K_\perp$ and $K_\parallel$ as given by Eqs. (10) and (11). The intermediate curves represent angles of 15°, 30°, 45°, 60°, and 75°, as determined from Eq. (7). The data points are from crystals oriented at 0° (○), 14° (▼), 28° (◇), 46° (□), 61° (◆), 75° (△), and 90° (●).

dicted by Eq. (7), indicates that this assumption
is valid for our 85-atm data. Nonetheless, it
would be useful to have our identification verified
by an x ray or birefringence experiment.[16]

We may interpret the qualitative dependence of
K on θ in terms of the phonon spectrum of the
solid. We suggest that parallel to the c axis the
phonon spectrum near the Brillouin-zone bound-
ary rises to about 18–27°K, whereas perpendic-
ular to the c axis the phonons near the Brillouin-
zone boundary have energies on the order of
30–45°K. These results are qualitatively in
agreement with the predictions of Nosanow and
Werthamer[17] for the velocities of sound in hcp
He⁴ crystals of 250 m/sec parallel to the c axis
and 305 m/sec perpendicular to it. Coupled with
our estimates of the Brillouin-zone boundary
behavior, this means a not unusual phonon spec-
trum.

Our data at 53.4 and 125.8 atm are not as ex-
tensive as the 85-atm data, and do not cover the
full range of crystal orientations expected from
Eq. (7), as we did not obtain two limit curves
giving a straight line in log$K$ versus $1/T$ at
either pressure. Slopes of all umklapp curves
at these pressures were consistent with the con-
clusion that the exponents in

$$K_{U\perp} = A_\perp e \, \exp(\Theta_D/b_\perp T) \qquad (12)$$

and $\quad K_{U\parallel} = A_\parallel e \, \exp(\Theta_D/b_\parallel T) \qquad (13)$

scale directly with Θ_D, i.e., that $b_\perp$ and $b_\parallel$ are
independent of pressure. Values of b were de-
termined to be $b_\perp = 2.58$ and $b_\parallel = 4.62$ from the
85-atm data. Ranges of the slopes at 53.4 and
125.8 atm suggest that most of the 53.4-atm
crystals were grown at low angles, and that most
of the 125.8-atm crystals were grown at high
angles. This is in agreement with expectations,
as 85-atm crystals grown at similar rates of
solidification (less than 1 cm/h for the 53.4-atm
crystals and 2-3 cm/h for the 125.8-atm crys-
tals) displayed similar ranges of preferred ori-
entation. Comparison of the magnitudes of K at
the same Θ/T but at different pressures show
that $A_\perp$ and $A_\parallel$ increase with increasing pressure,
but the data are too few to permit any quantitative
observations on the pressure dependence of $A_\perp$
and $A_\parallel$. A probable 0° crystal (Run 8-1) at 53.4
atm indicates that $A_\parallel (53.4\,\text{atm}) \cong 0.61 A_\parallel$ (85 atm);
the 125.8-atm curves suggest that $A_\perp(125.8\,\text{atm})$
may be $\cong 3/2 A_\perp$(85 atm), but these numbers and
identifications should be confirmed by a complete
study of $K(\theta, T)$ and $\bar{K}$ at these pressures before
being considered reliable.

B. Geometrical Region

The geometrical region of the thermal conduc-
tivity includes the boundary and Poiseuille-flow
regions discussed in Sec. II. Low umklapp con-
ductivities at 53.4 atm resulted in very low-
temperature peaks in the K-versus-T curve, and
no useful information was obtained on geometri-
cally limited conductivity at this pressure. At
85 and 125.8 atm, however, data were obtained
on both the boundary-limited and Pouiseuille-flow
regions, although the transition between them
lies nearly at the low-temperature limit of our
apparatus at these pressures. Not all crystals
displaying good (unsplit) umklapp conductivities
could be used for analysis in these regions, as a
crystal with a good umklapp conductivity some-
times displayed a split boundary and/or Poiseuille
region. The Poiseuille region was the most
prone to splitting, as expected by the relative
effect of small amounts of defects on a boundary-
limited and a Poiseuille-flow mean free path.
Small differences (less than 10%) in the conduc-
tivity of the two halves of a given crystal were
usually present at some temperatures in even the
best crystals, usually at and just below the peak
in the K-versus-T curve. For this reason only
crystals with conductivities matched to within
10% throughout the temperature range were se-
lected for analysis, and only the best half of each
crystal was used. While this procedure cannot
guarantee that a small uniform concentration of
defects may not still affect the results, it does
tend to eliminate crystals containing localized
concentrations of defects and crystals with large
numbers of defects. It was noted that, at a given
pressure, crystals meeting the above criterion
also agreed well with each other in the geometri-
cal region, despite large variations in the um-
klapp conductivity, whereas crystals showing
splits invariably displayed lower geometrical K-
versus-T curves than the values given by unsplit
crystals. The differences in boundary-limited
thermal conductivity between good crystals of
varying orientation may be accounted for by the
prediction of Eq. (9) that K in the boundary region
goes as c_a^{-2}. The relation $K_\perp > K_\parallel$ in the umklapp
region implies that $c_\perp > c_\parallel$, in agreement with
Nosanow and Werthamer,[17] which implies that the
boundary $K_\perp$ should be less than the boundary $K_\parallel$.
This prediction is borne out by the data in Fig. 3,
as all the crystals presented are considered to be
good single crystals. This relationship is also
qualitatively obeyed by the data on good crystals
at 125.8 atm, although the range of angles is much
smaller in this case.

Finally, we note that the anisotropy in the bound-
ary region is very mild, particularly when com-
pared with the umklapp anisotropy of the same
crystals. This anisotropy at the lowest tempera-

tures is consistent with the expectations given above, but this fact could be fortuitous in view of the possibility that small amounts of defects may remain in some or all of these crystals.

In Fig. 6 we show the data on crystal 11-12 ($d = 2.68$ mm, $\theta = 90°$) in the geometrical region on a $\log K$-versus-$\log T$ plot. The curve shows two distinct slopes, with a slope of 3 at the lowest temperatures and a slope of about 6 at temperatures just below T_{max}, the temperature at which the peak of the thermal conductivity curve occurs. The thermal conductivity at the lowest temperatures approaches the prediction of Eq. (1) using the Debye sound velocity, as expected in the boundary region. The increased slope in the K-versus-T curve below T_{max} is characteristic of Poiseuille flow. A $\log K$-versus-$\log T$ plot was prepared for each crystal to determine the temperature dependence of the Poiseuille-flow thermal conductivity, and straight-line fits to the Poiseuille-flow data were made to determine the exponent N in the expression $K \alpha T^N$. A value of $N = 5.75 \pm 0.35$ was found to cover both halves of all good single crystals (unsplit in the geometrical region) grown in the 2.68-mm-diam sample chamber, with the higher values of N occurring at the higher orientation angles θ, where the Poiseuille region in the data covers a larger temperature range. Lower values of N were observed in the smaller chamber, where low orientation angles and low boundary-limited conductivities combined to interfere with the Poiseuille-flow mechanism.
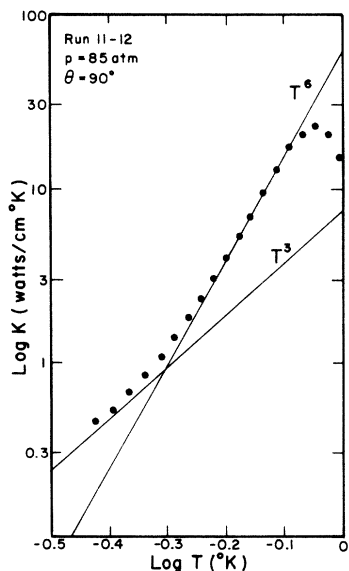
For crystals where Poiseuille flow is the dominant mechanism in determining K in some temperature region, it is possible to apply Eq. (2) to the K data for the Poiseuille region and determine τ_N and λ_N. Results of this analysis using the parameters of Table I are presented in Table II. We find that the data on crystals exhibiting a definite Poiseuille-flow region (those grown in the large sample chamber) can be represented by

$$\lambda_N(T, 85 \text{ atm}) = (4.0 \pm 1.0) \times 10^{-3} T^{-3} \text{ cm} \quad (14)$$

at 85 atm, and by

$$\lambda_N(T, 126 \text{ atm}) = (7.7 \pm 0.7) \times 10^{-3} T^{-3} \text{ cm} \quad (15)$$

at 126 atm. These results are in good agreement with the estimates of $\lambda_N(T)$ obtained from the analysis of second sound data and Mezhov-Deglin's Poiseuille-flow data by Ackerman and Guyer.[18] These authors obtain the rule

$$\tau_N(T) = 2 \times 10^{-12} (\Theta_D/T)^3 \text{ sec.} \quad (16)$$

At 85 atm this formula gives $\lambda_N = c \tau_N(85 \text{ atm})$ $= 3.8 \times 10^{-3} T^{-3}$ cm, and at 126 atm $\lambda N = c^T N(126$ atm)$= 6.7 \times 10^{-3} T^{-3}$ cm. The present data can be represented by

$$\tau_N(T) = (2.1 \pm 0.4) \times 10^{-12} (\Theta_D/T)^3 \text{ sec.} \quad (17)$$

There is no question that the present data are far better than those available to Ackerman and Guyer. Thus it is best to regard this earlier result as lending support to the above calculations rather than vice versa. The determination of $\tau_N(T)$ by Ackerman and Guyer relied very heavily on the second-sound data. The confirmation of that determination by the present experiment lends strong support to the view taken by Ackerman and Guyer in their analysis.

We further note that over the limited range of pressures explored in this experiment the scaling of τ_N with Θ_D^3 is verified.

In Fig. 7 we have plotted $\tau_N = \lambda_N/c$ from several crystals at 85 and 126 atm as a function of the angle θ defined by the behavior of K in the umklapp region. The 126-atm data, which are on large-angle crystals, are plotted as open triangles. The 85-atm data in the large sample chamber are plotted as closed circles; the 85-atm data in the small sample chamber are plotted as open circles. Note that Poiseuille flow is not fully developed for the points representing data in the small chamber, as K versus T never exceeds about T^5 for curves taken in this chamber. There is some slight evidence in this plot for an angular dependence to τ_N. On the other hand, the velocity of sound is known to be at least as anisotropic as the effect

FIG. 6. Thermal conductivity of Run 11-12, $\theta = 90°$. The T^6 line is fitted to the data points; the T^3 line is calculated for the boundary region assuming a Debye velocity of sound.

TABLE I. Parameters used in analyzing the data. The values of molar volume and of Θ_D are taken from D. O. Edwards and R. C. Pandorf, Phys. Rev. 140, A816 (1965). The values for the velocity of sound are calculated from $c_D = K_B \Theta_D / (6\pi^2 N)^{1/3} \hbar$, where N is the number of atoms per unit volume.

Growth pressure (atm)	53.4	85.0	125.8
Molar volumes (cm³/mole)	19.47	18.31	17.36
Θ_D(°K)	31.7	36.7	42.4
Debye sound velocity (m/sec)	338	384	436

TABLE II. Poiseuille-flow results. The values of λ_0, λ', and τ' are obtained from the equation $\lambda_N(\Theta_D, T) = \lambda_0/T^3$ $= \lambda'(\Theta_D/T)^3 = c_D\tau'(\Theta_D/T)^3$, where $\tau_N(\Theta_D, T)$ is obtained from Eq. (2). "Graph error" represents the estimated uncertainty in choosing the Poiseuille region values of K/T^6 from graphs of K/T^6 versus T.

Run	Angle (deg)	K/T^6 [W/cm(°K)⁷]	λ_0 (10⁻³ cm)	λ' (10⁻⁸ cm)	τ' (10⁻¹² sec)	Graph error (%)	λ Peak (cm)	λ BDY (cm)
9-7[a]	28	40.7	3.32	6.72	1.75	2.5	0.457	0.240[b]
10-23[a]	38	41.0	3.30	6.68	1.74	2.4	0.477	0.225
10-24[a]	36	40.7	3.32	6.72	1.75	1.7	0.466	0.227
11-1	7	80.0	3.87	7.83	2.04	2.5	0.784	0.315
11-3	61	77.6	3.99	8.07	2.10	1.9	1.016	0.331
11-4	14	80.0	3.87	7.83	2.04	1.2	0.802	0.326
11-7	82	71.5	4.33	8.76	2.28	2.1	1.277	0.289
11-12	90	61.7	5.01	10.13	2.64	1.0	1.201	0.291
11-14	78	31.2	7.70	10.10	2.32	1.0	1.111	0.296
11-15	85	28.7	8.37	10.98	2.52	2.8	1.116	0.287
11-18	72	34.3	7.01	9.20	2.11	0.9	1.110	0.303
11-19[c]	72	32.8	7.34	9.63	2.21	1.5	1.019	0.295

[a]Poiseuille flow not fully developed for these runs, made in small sample chamber. Lack of fill capillary correction leads to erroneously high λ BDY's.

[b]Boundary region not reached in this run.

[c]This crystal may have a small concentration of defects.
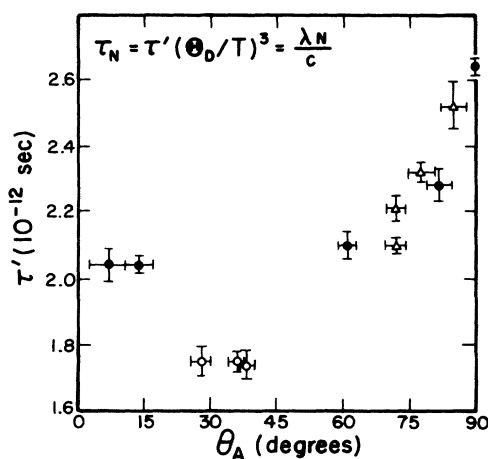
FIG. 7. Normal-process collision times. Note that Poiseuille flow is not fully developed in the three runs represented by open circles. The error bars represent graphical uncertainties in selecting θ and K/T^6 from the data rather than errors in individual data points.

we observe. Since we have made on effort to acknowledge this anisotropy in our calculations, we do not feel that we can draw any conclusion about the anisotropy in τ_N. Residual defects may be present in some or all of these crystals, and if present would result in apparent values of τ_N higher than the true values.

In Fig. 8 we have plotted the K data in the geometrical region from crystals grown at 85 atm in sample chambers of two different sizes. The open circles are data on a sample chamber 1.77 mm in diameter; the closed circles are data on a sample chamber 2.68 mm in diameter. In Fig. 8 we have also plotted two auxiliary curves. The open triangles in Fig. 8 are the data on the smaller sample chamber scaled up by the ratio of the sample chamber diameters, $(d_>/d_<) = (2.68/1.77)$ $= 1.51$. The closed triangles in Fig. 8 are the data on the smaller sample chamber scaled up by the ratio of the diameters squared, $(d_>/d_<)^2$ $= (2.68/1.77)^2 = 2.29$. We note that at lowest temperatures the data on the two sample chambers scale as d. At temperatures near T_{max} they
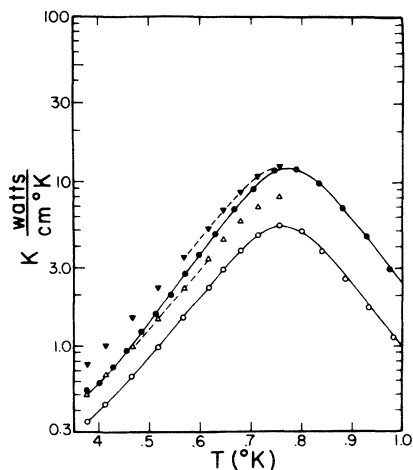
FIG. 8. Dependence of thermal conductivity on sample chamber dimensions. $\bigcirc$ — Run 10-24, $d_< = 0.1773$ cm.
$\bullet$ — Run 11-3, $d_> = 0.2682$ cm. ∇ — (Run 10-24) $\times$ $(d_>/d_<)$.
$\blacktriangledown$ — (Run 10-24) $\times$ $(d_>/d_<)^2$.

FIG. 9. Experimental mean free paths at 85 atm in large chamber.

scale as d^2. This result is a confirmation of the d^2 dependence of K in the Poiseuille-flow region [Eq. (2)].

It should be noted at this point that the possibility exists that Poiseuille flow is not fully developed in our larger sample chamber ($d = 2.68$ mm), and that repetition of this experiment with larger or higher-quality crystals might lead to higher values of $K \propto T^N$ than $N = 6$, as claimed by Mezhov-Deglin[6] and predicted by Herring.[19] While this possibility cannot be entirely ruled out, a number of points seem to indicate that this is not the case. Our 2.68-mm-diam sample chamber is larger than the 2.47-mm-diam chamber for which Mezhov-Deglin reports his results. Our data are highly consistent, both between halves of the same crystal and from run to run in those crystals believed to be good single crystals (see the Appendix and Fig. 3). Our data are also quantitatively supported by the second-sound results of Ackerman and Guyer which were obtained in sample chambers with smallest dimensions of 7.7 mm or larger in which there were single crystals filling most of their volume. Our large sample chamber also seems to produce crystals of minimum dimension approximately equal to the sample chamber diameter as discussed below.

In Figs. 9 and 10 we have plotted the thermal conductivity mean free path, defined by

$$\lambda_K = 3K/C_v c , \qquad (18)$$

as a function of T for four crystals grown at 85 atm in the large sample chamber, Fig. 9; and four crystals grown at 126 atm in the large sam-

ple chamber, Fig. 10. The common characteristic of these plots is that at lowest temperatures λ_K is approximately d (see Table II). This result is very satisfying in that it strongly suggests that the low-temperature thermal conductivity is limited by the sample chamber boundary and not by some crystallite dimension. The crystals fill the sample chamber singly in the transverse direction and have a length at least equal to the diameter of the sample chamber. At temperatures near T_{max} we find thermal conductivity mean free paths of several centimeters (see Table II). For example, in the 90° crystal at 85 atm in the large sample chamber, λ_K is approximately 1.5 cm.
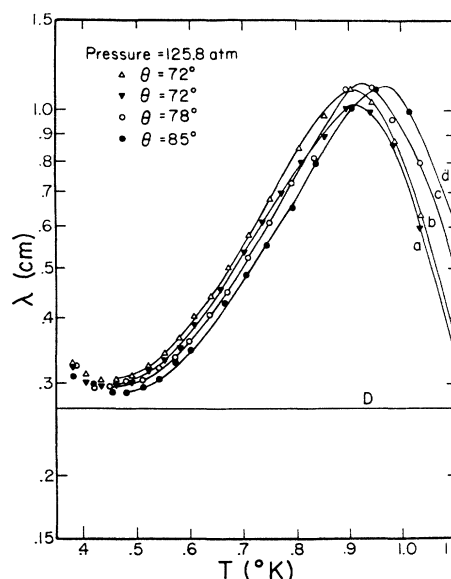
FIG. 10. Experimental mean free paths at 125.8 atm in large chamber.

This means that the crystals we have grown are at least 1.5 cm long. Further the fact that the umklapp conductivity is unsplit suggests that they may be at least as long as the spacing between the extreme thermometers, approximately 5 cm. Mezhov-Deglin's best crystal MD-I has a maximum mean free path of about 1 cm (see Fig. 3 of Ref. 6). It is clear from Fig. 9 that the amount of Poiseuille region observed for a given crystal depends strongly on angle, hence our most recent efforts have been directed toward growing high-angle crystals.

In Fig. 11 we have shown an experimental mean-free-path diagram.

We note that the T^3 temperature dependence which we find for τ_N^{-1} does not agree with the expectations of theory. For example, for

$$|V^{(3)}|^2 \propto |\vec{q}_1| |\vec{q}_2| |\vec{q}_3| \delta(\vec{q}_1 + \vec{q}_2 + \vec{q}_3), \qquad (19)$$

where $V^{(3)}$ is the cubic anharmonic coefficient in the potential energy, we have $\tau_N^{-1} \propto T^5$.[20] We have oriented our efforts in this paper toward a quantitative description of the results of the experiment. The description has been in terms of the relatively simple view of the heat transport process which is summarized in the equations of Sec. II. Within this framework we find $\tau_N^{-1} \propto T^3$. This is the strongest claim we would like to make in this paper. We are somewhat puzzled by this result. But (a) we are not sure that in a quantum solid the three-phonon process obeys Eq. (19) and/or that only it contributes to τ_N^{-1}, and (b) we would not be surprised if as Poiseuille flow approaches boundary scattering a modification must
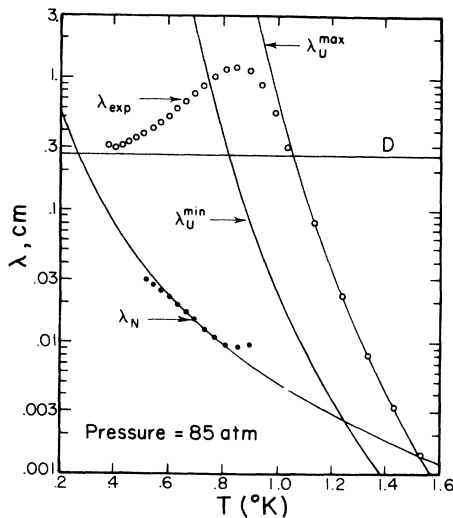
be made of the physical explanation of the conductivity process, i.e., Eq. (2) must be modified. Thus our present view is that the T^3 which we have obtained is by far the soundest piece of information presently available on the behavior of τ_N^{-1}.

C. Peak Region

In the preceding, we have dealt with each mechanism controlling the thermal conductivity in a region of the experimental data in which the mechanism in question is dominant. The next logical step is to attempt to construct theoretical fits to the data in the region where more than one mechanism may be important in determining the thermal conductivity. Since the bulk of our temperature range lies in the region where the Ziman limit ($\lambda_N \ll \lambda_R$) is valid, we shall present the results of fitting our data to Eq. (4). This procedure is valid for predicting thermal conductivity values over the peak of the K-versus-T curve.

We have used Eq. (4) to calculate $K(T)$ at 85 atm: (1) for a 90° crystal in our large sample chamber, $d = 2.68$ mm, and (2) for a 90° crystal in Mezhov-Deglin's small sample chamber,[7] $d = 1.60$ mm. To perform these calculations we use Eq. (2) in the form

$$K_P = \tfrac{5}{96} C_v d^2 / \tau_N . \qquad (20)$$

Note that μ in the $G(\mu)$ term is now given by

$$\mu = 2K_P/K_Z , \qquad (21)$$

where K_Z is given by Eq. (3), and that Eqs. (10) and (11) permit the calculation of K_Z for any temperature and crystal orientation.

For the 90° calculations we have used $K_Z = K_\perp$ as given by Eq. (10). For K_P at 90° we have

$$K_P(90°) = 860 d^2 T^6 \text{ W/cm °K} . \qquad (22)$$

The results of these calculations are shown in Fig. 12 as the solid curves labeled 1 and 2. As expected, the two 90° curves (1 and 2) tend to mesh at high temperatures. At low temperatures the 90° curves are related by a factor of $(2.68/1.60)^2$. The dashed curve 1′ represents K_Z alone for $\theta = 90°$.

On the same figure we have plotted a number of sets of experimental data; our curve 11-12 ($\theta = 90°$) and the curves labeled "a" and "b" from Fig. 2 of Mezhov-Deglin (Ref. 7). The notable features of the theoretical curves are:

1. The data from Run 11-12 (the closed circles) fits the theoretical curve $K(2.68$ mm, 90°) very well over the peak. It is expected to fit well at

FIG. 11. Experimental mean free paths at 85 atm. Data points for λ_{expt} are from crystal 11-12, $\theta = 90°$. D is sample chamber diameter. The λ_U lines are from Eq. (10) and (11). The λ_N line is from Eq. (14).
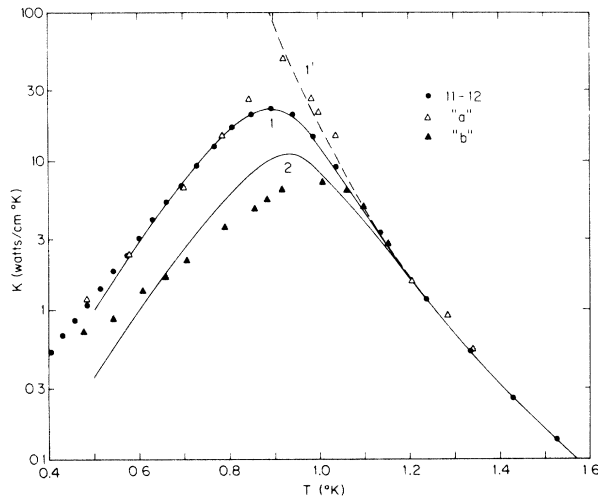
FIG. 12. Fitting of thermal conductivity data over peak of curve. Dashed curve 1' is from Eq. (10). Solid curves are obtained from Eq. (4) as described in the text.

high and low temperatures, since this data supplied the parameters used in constructing the curve, but the fit over the peak suggests both that the Ziman limit equation (4) is correct, and that our data are consistent with it. If the data near the peak were depressed because of the presence of isotopic or chemical impurities, K computed from Eq. (4) would rise above the experimental curve. We take the agreement of the experimental and computed curves near the peak as evidence that there is no significant concentration of impurities or defects in the sample. Similar computations were made for our other good 85-atm crystals using values of Kp obtained from the low-temperature data on each curve, and similar agreement was obtained between theory and experiment over the peaks of the curves.

2. The data from Mezhov-Deglin's "a" crystal (the open triangles) are those of his "best of group I" crystal, and go far above the computed curve over the peak. The computed curve 1 has a maximum conductivity of about 23 W/cm°K as do our data. Mezhov-Deglin's crystal, having a diameter of 2.47 mm compared with our 2.68 mm, has a peak conductivity of about 50 W/cm°K. Since the low-temperature points for Mezhov-Deglin's crystal lie close to ours, and the umklapp curves should be identical for the same growth pressure, we would expect his data to yield a calculated curve very similar in magnitude and peak shape to ours. Thus a discrepancy exists between Mezhov-Deglin's "a" crystal data and the prediction of Eq. (4).

3. The data from Mezhov-Deglin's crystal "b" (closed triangles) should follow curve 2, since it is a 90° crystal in a 1.60-mm sample chamber.

The data seem to follow the curve above T_{max}, but fall below curve 2 below the peak. Quite probably this is due to defects remaining in the crystal.

As a consequence of this analysis, we believe that while the data of Mezhov-Deglin may be qualitatively correct, they cannot be used for detailed quantitative analysis. We also believe that the data from the present experiment are internally self-consistent and of sufficient quantitative accuracy to permit some confidence in the numerical results presented in the previous sections.

There is an alternative way to represent these results. By calculating $K(T, d, \theta)$ from Eq. (4), it is possible to get K_{max} as a function of T_{max} for fixed d and varying θ. Such a curve is shown in Fig. 13. The five crystals of $d = 2.68$ mm, pressure = 85 atm, that we have used as good single crystals have their K_{max}-T_{max} regions indicated by the dark areas. A region is required because K_{max}-T_{max} is not a single point unless the crystal is absolutely unsplit, and even our "good" single crystals can display slight splits at the peak of the K-versus-T curve. These dark areas fall on the K_{max}-T_{max} line computed from Eq. (4). It is suggested that such a curve is a simple test of crystal quality. Those of our crystals that for one reason or another we do not classify as good single crystals have K_{max}-T_{max} regions lying below this line. On the same figure we have indicated the K_{max}-T_{max} points for each of the five crystals discussed by Mezhov-Deglin (Ref. 7), and none of them fall near the appropriate line.
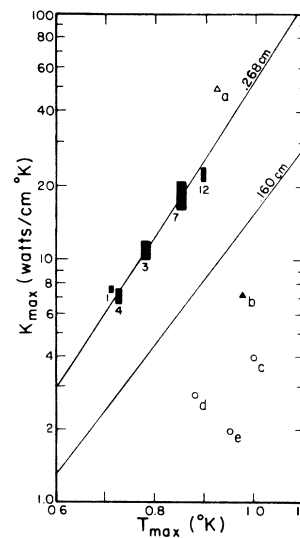
FIG. 13. K_{max} versus T_{max} for varying orientation θ at 85 atm. The solid rectangles are the peak regions of our good single crystals grown at 85 atm. The lettered points are the 85-atm crystals of Mezhov-Deglin (Ref. 7).

D. Comparison with Mixture Results

Recently, there have been four separate attempts to employ the Callaway equation[21] to analyze thermal conductivity data on solid He^3-He^4 mixtures.[14, 22-24] Since the lattice distortion + mass fluctuation[25] scattering cross section σ is not known, the analysis must fix one more than the usual number of parameters. The steps followed are: (1) Data on an isotopically and chemically pure crystal are analyzed to find consistent sets of parameters which characterize normal process and umklapp process scattering; (2) Further data on isotopically disordered solid mixtures are analyzed to fix the set of N-process and U-process parameters and the strength of the mass fluctuation + lattice distortion scattering. Rogers et al.[22] have analyzed data on four concentrations, each at filling pressures of 60, 90, and 140 atm. They found for all three pressures

$$\tau_N(T) \approx 5 \times 10^{-15}(\Theta_D/T)^4 \text{ sec.} \tag{23}$$

Bertman et al.[15] analyzed mixture data on five concentrations at 19.5 cm^3/mole (thus the pressure varies with concentration) and found

$$\tau_N(T) \approx 2 \times 10^{-15}(\Theta_D/T)^5 \text{ sec.} \tag{24}$$

Agrawal[24] has analyzed the 20.2-cm^3/mole data of Bertman et al. He finds

$$\tau_N(T) \approx 2 \times 10^{-15}(\Theta_D/T)^5 \text{ sec.} \tag{25}$$

Most recently, Berman et al.[23] have analyzed measurements on mixtures at four higher pressures, 190, 250, 800, and 1725 atm; they find

$$\tau_N(T) \approx 3 \times 10^{-16}(\Theta_D/T)^5 \text{ sec.} \tag{26}$$

From the point of view of mass defect scattering, the recent results of Berman et al. are most satisfactory. They find that as the pressure of the solid is raised, the strength of the mass fluctuation + lattice distortion scattering approaches the strength expected for mass fluctuation scattering alone. Their results are in excellent qualitative agreement with the prediction by Klemens et al.[26] They are in good quantitative agreement with a recent calculation of Guyer.[27]

Three independent direct measurements of τ_N have been made. (1) The data of Mezhov-Deglin on Poiseuille flow in sample chambers of several diameters and at four pressures.[5-7] (2) The second-sound data of Ackerman and Guyer.[18] (3) The Poiseuille-flow measurement discussed above. The data of Mezhov-Deglin and Ackerman and Guyer have been analyzed in Ref. 18 and $\tau_N(T)$

was determined to be given by

$$\tau_N(T) = 2 \times 10^{-12}(\Theta_D/T)^3 \text{ sec.} \tag{27}$$

The data exist in the temperature range $1.2 \times 10^{-2} \leq T/\Theta_D \leq 2 \times 10^{-2}$, and therefore fix τ_N at $T \approx 0.6$ to $0.8°$K at a pressure of 85 atm. The present experiment yields

$$\tau_N(T) = (2.1 \pm 0.4) \times 10^{-12}(\Theta_D/T)^3 \text{ sec}, \tag{28}$$

which is in good agreement with the result above, Eq. (27).

Thus the magnitude of $\tau_N(T)$ at temperatures just below the low-temperature maximum is well established. The dependence on $(\Theta_D/T)^3$ is consistent with the data, but not defined by it.

None of the $\tau_N(T)$ from the Callaway analysis of mixture data agree with the direct determination of $\tau_N(T)$. The recent results of Berman et al. most closely approach the directly measured values in the relevant T range.

We have employed the Callaway equation in an attempt to fit the mixture data at 140-atm filling pressure of Rogers et al.[22] using $\tau_N(T)$ as determined by us above. In this analysis, the form of the Callaway equation suggested by Guyer and Krumhansl[2] was used, i.e.,

$$K = \frac{1}{3} C_v c^2 \left[\tau_R^K \left(\frac{S}{1+S} \right) + \tau_R^Z \left(\frac{1}{1+S} \right) \right], \tag{29}$$

where $\tau_R^{-1} = \tau_U^{-1} + \tau_I^{-1} = A\omega^4$ is the mass fluctuation + lattice distortion scattering rate and $S = \tau_N(T)/\tau_R^K$. Now

$$\tau_R^K = \int_0^\infty A(x)\tau_R(x)dx / \int_0^\infty A(x)dx,$$

and

$$\tau_R^Z = \left(\int_0^\infty A(x)dx / \int_0^\infty A(x)\tau_R(x)^{-1}dx \right)^{-1},$$

where $A(x) = x^4 e^x/(e^x + 1)^2$ and $x = \hbar\omega/K_B T$. We may therefore use the experimentally determined $\tau_N(T)$ directly in the analysis without having to unravel its ω and T dependence. Further, we have used the polycrystalline average of the umklapp scattering rates, since the samples studied by Rogers et al. were formed by the blocked capillary technique. In particular, we took

$$\tau_U(\omega, T) = \frac{3\tau_\perp(\omega, T)\tau_{||}(\omega, T)}{2\tau_{||}(\omega, T) + \tau_\perp(\omega, T)},$$

where

$$\tau_\perp(\omega, T) = 1.82 \times 10^{-11} \frac{1}{T^3} \frac{1}{x^2} e^{14.2°K/T} \text{ sec},$$

and

$$\tau_{\parallel}(\omega, T) = 1.05 \times 10^{-10} \frac{1}{T^3} \frac{1}{x^2} e^{7.9°K/T} \text{sec},$$

T being in $°K$.

The results of this analysis were not entirely satisfactory. The data at $T < 2°K$ were fit reasonably well for a scattering strength having the correct concentration dependence, but about an order of magnitude greater than that found by Berman *et al*. However, this scattering strength was about a factor of 2 too strong to fit the data at $T > 2°K$. In the range $T < 2°K$, the fit was of the same quality as that found by Agrawal for the 20.2-cm³ mole data.

We have also attempted to fit the mixture data by inserting an extra factor $(0.7/T)^n$ in Eq. (28) for $\tau_N(T)$, on the assumption that the Poiseuille-flow data, although they give the correct magnitude for $\tau_N(T)$, do not display the correct temperature dependence. All of the higher-power laws, T^{4-5}, yield far worse fits than the T^3 from Eq. (27).

As a consequence of the unsatisfactory nature of these attempts to fit the mixture data, we must conclude that we are unable to reconcile $\tau_N(T)$ obtained from Poiseuille-flow measurements with the Callaway analysis of the mixture data.

E. Comparison with bcc He³

We have shown that the thermal conductivity of hcp He⁴ in the umklapp region is highly anisotropic and must be described by the tensor

$$\tilde{K}_{\text{hcp}} = \begin{pmatrix} K_{\perp} & 0 & 0 \\ 0 & K_{\perp} & 0 \\ 0 & 0 & K_{\parallel} \end{pmatrix}, \quad (30)$$

where $K_{\perp}^{-1} = A_{\perp} \exp(-a_{\perp}/T)$ and $K_{\parallel}^{-1} = A_{\parallel} \exp(-a_{\parallel}/T)$, $A_{\perp} = 9 \times 10^4$, $A_{\parallel} = 4 \times 10^3$, $a_{\perp} = 14.2$, $a_{\parallel} = 7.9$ for a crystal grown at a constant pressure of 85 atm.

The anisotropy of the thermal conductivity of hcp He⁴ is explained microscopically by noting that: (a) The thermal conductivity is proportional to an average of the umklapp scattering rate

weighted in the direction of the heat current by a factor $\cos^2\theta$; (b) there are essentially two groups of phonons participating in the conduction process, a high-energy group and a low-energy group. When the heat current is propagated perpendicular to the c axis, the spatial weighting favors the high-energy phonon group; heat currents parallel to the c axis are carried by the low-energy phonon group.

The phonon spectrum of bcc He³ is like that of other bcc crystals.[17] Thermal conductivity of bcc He³ is *not* anisotropic, since the crystal is cubic. Nonetheless we suggest that two groups of phonons participate in the conduction process independent of the direction of the heat current. Since the Ziman limit obtains for the conduction process, the two groups of phonons contribute to the thermal resistivity additively

$$K_{\text{bcc}}^{-1} = K_>^{-1} + K_<^{-1}. \quad (31)$$

In analogy to the hcp case, we write for each group, $K_{>,<}^{-1} = A_{>,<} \exp(-a_{>,<}/T)$. Bertman *et al*.[14] have analyzed their bcc He³ thermal conductivity data using Eq. (30), and find $K_>^{-1} = 2 \times 10^5 \exp[-(14/T)]$ and $K_<^{-1} = 2 \times 10^3 \exp[-(4/T)]$.

There exist in the phonon spectrum of hcp He⁴ variations (i.e., two phonon groups) which give rise to $K_{\perp}$ and $K_{\parallel}$ of Eq. (30). It is not unlikely that qualitatively similar variations occur in the phonon spectrum of bcc He³ which give rise to $K_>$ and $K_<$ of Eq. (31). We take the quantitative agreement, $A_< \approx A_{\parallel}$ and $A_> \approx A_{\perp}$ and $a_< \approx a_{\parallel}$ and $a_> \approx a_{\perp}$ as evidence that this assertion is correct.

ACKNOWLEDGMENTS

APPENDIX

The following tables contain representative data from which the numbers in Table II and the conclusions in the text were obtained.

Run 8-1		Run 10-2		Run 10-10	
Sample diameter 0.1773 cm, growth rate < 1 cm/h, growth pressure 53.4 atm, orientation angle 0°.		Sample diameter 0.1773 cm, constant volume growth, molar volume 18.31 cc/mole, polycrystalline sample.		Sample diameter 0.1773 cm, growth rate 3.00 cm/h, growth pressure 85 atm, orientation angle 0°.	
K (W/cm °K)	T (°K)	K (W/cm °K)	T (°K)	K (W/cm °K)	T (°K)
0.0073	1.733	0.076	1.528	0.038	1.563
0.0096	1.630	0.115	1.427	0.054	1.463
0.0121	1.555	0.185	1.330	0.081	1.363
0.0179	1.430	0.306	1.234	0.129	1.262
0.0254	1.331	0.540	1.136	0.227	1.158
0.0383	1.233	0.966	1.040	0.436	1.055
0.0620	1.136	1.27	0.993	0.629	1.003
0.107	1.042	1.61	0.946	0.919	0.951
0.198	0.952	1.90	0.900	1.37	0.899
0.278	0.909	2.03	0.856	1.95	0.850
0.407	0.865	1.96	0.813	2.42	0.804
0.631	0.818	1.76	0.774	2.55	0.760
0.882	0.783	1.51	0.738	2.32	0.720
1.36	0.738	1.17	0.686	1.91	0.684
1.77	0.704	0.973	0.653	1.57	0.652
2.12	0.670	0.818	0.623	1.29	0.624
0.952	0.775	0.705	0.598	1.08	0.600
1.84	0.698	0.591	0.570	0.740	0.548
2.26	0.635	0.506	0.542	0.502	0.497
2.08	0.605	0.413	0.512	0.337	0.443
2.04	0.598	0.333	0.478	0.242	0.396
		0.279	0.451	0.192	0.364
		0.214	0.412		
		0.189	0.392		
		0.162	0.369		

Run 11-1		Run 11-3		Run 11-4	
Sample diameter 0.2682 cm, growth rate 1.3 cm/h, growth pressure 85 atm, orientation angle 7° ± 4°.		Sample diameter 0.2682 cm, growth rate 2.2 cm/h, growth pressure 85 atm, orientation angle 61° ± 2°.		Sample diameter 0.2682 cm, growth rate 1.5 cm/h, growth pressure 85 atm, orientation angle 14° ± 3°.	
K (W/cm °K)	T (°K)	K (W/cm °K)	T (°K)	K (W/cm °K)	T (°K)
0.044	1.528	0.090	1.527	0.045	1.529
0.064	1.428	0.148	1.427	0.065	1.429
0.096	1.331	0.251	1.330	0.099	1.331
0.155	1.233	0.454	1.233	0.160	1.233
0.283	1.130	0.901	1.132	0.290	1.131
0.562	1.031	1.95	1.030	0.581	1.032
0.839	0.982	3.00	0.979	0.848	0.984
1.29	0.934	4.62	0.931	1.31	0.936
2.08	0.884	6.92	0.883	2.12	0.886
3.44	0.835	9.83	0.837	3.47	0.837
5.45	0.786	11.9	0.790	5.44	0.788
7.23	0.742	11.7	0.747	7.20	0.744
7.37	0.699	8.96	0.705	7.63	0.702
6.09	0.659	6.76	0.666	6.36	0.662
4.51	0.621	4.79	0.631	4.74	0.625
3.32	0.587	3.61	0.599	3.46	0.592
2.09	0.540	2.72	0.571	2.79	0.570
1.34	0.493	2.05	0.541	2.09	0.541
0.873	0.447	1.57	0.513	1.58	0.513
0.606	0.402	1.21	0.485	1.24	0.485
0.467	0.378	0.929	0.457	0.956	0.457
		0.733	0.430	0.740	0.430
		0.599	0.403	0.634	0.405
		0.534	0.377	0.486	0.378

Run 11-7		Run 11-12		Run 11-18	
Sample diameter 0.2682 cm, growth rate 2.76 cm/h, growth pressure 85 atm, orientation angle 82° ± 3°.		Sample diameter 0.2682 cm, growth rate 3.5 cm/h, growth pressure 85 atm, orientation angle 90°.		Sample diameter 0.2682 cm, growth rate 1.43 cm/h, growth pressure 125.8 atm, orientation angle = 72°.	
K (W/cm °K)	T (°K)	K (W/cm °K)	T (°K)	K (W/cm °K)	T (°K)
0.130	1.527	0.137	1.529	0.540	1.529
0.239	1.427	0.258	1.429	1.01	1.429
0.470	1.330	0.524	1.334	1.93	1.333
1.03	1.233	1.18	1.239	3.95	1.230
2.55	1.132	3.30	1.136	8.34	1.129
6.36	1.035	9.25	1.037	15.2	1.033
9.99	0.985	14.7	0.988	16.7	0.987
14.7	0.939	20.5	0.942	17.3	0.942
19.8	0.894	22.7	0.896	14.7	0.898
21.0	0.850	20.4	0.851	12.3	0.855
18.4	0.806	17.0	0.808	8.44	0.804
14.3	0.766	12.6	0.768	5.63	0.748
10.7	0.727	9.41	0.729	4.04	0.706
7.96	0.691	6.84	0.694	2.97	0.668
5.75	0.659	5.34	0.662	2.23	0.632
4.39	0.629	4.01	0.629	1.73	0.600
3.35	0.600	3.03	0.600	1.39	0.570
2.52	0.571	2.32	0.571	1.12	0.542
1.93	0.543	1.81	0.542	0.916	0.513
1.48	0.515	1.40	0.514	0.739	0.483
1.16	0.486	1.08	0.485	0.609	0.455
0.894	0.459	0.850	0.458	0.507	0.427
0.687	0.431	0.672	0.430	0.422	0.401
0.546	0.404	0.529	0.404	0.363	0.378
0.431	0.379	0.458	0.377		

[1]John Wilks, Liquid and Solid Helium (Clarendon Press, Oxford, England, 1967).

[2]R. A. Guyer and J. A. Krumhansl, Phys. Rev. 148, 778 (1966).

[3]R. A. Guyer and E. M. Hogan, Solid State Commun., 5, 909 (1967).

[4]A. I. Shalnikov, Zh. Eksperim. i Teor. Fiz. 41, 735 (1961) [English transl.: Soviet Phys. – JETP 14, 530 (1962)].

[5]L. P. Mezhov-Deglin, Zh. Eksperim i Teor. Fiz. 46, 1923 (1964) [English transl.: Soviet Phys. – JETP 19, 1297 (1964)].

[6]L. P. Mezhov-Deglin, Zh. Eksperim i Teor. Fiz. 49, 66, (1965) [English transl.: Soviet Phys. – JETP 22, 47 (1966)].

[7]L. P. Mezhov-Deglin, Zh. Eksperim. i Teor. Fiz. 52, 866 (1967) [English transl.: Soviet Phys. – JETP 25, 568 (1967)].

[8]A preliminary report of some of the results of this investigation is contained in Ref. 3.

[9]R. Peierls, Quantum Theory of Solids (Clarendon

Press, Oxford, England, 1955).

[10]We are employing the results of Ref. 2 in our discussion of thermal conductivity. Various aspects of this problem have been treated by others. For example: the phenomena of Poiseuille flow in a phonon gas were first suggested by J. A. Sussman and A. Thellung, Proc. Phys. Soc. (London) 81, 1122 (1963). N. Gurzi, Zh. Eksperim. i Teor. Fiz. 46, 719 (1964) [English transl. Soviet Phys. − JETP 19, 490 (1964)], has given a full treatment of Poiseuille flow and thermal conductivity at low temperatures.

[11]Warren P. Mason, Crystal Physics of Interaction Processes (Academic Press Inc., New York, 1966).

[12]P. Carruthers, Rev. Mod. Phys. 33, 92 (1961).

[13]G. McConville, R. Watkins, and W. Taylor, Physica Suppl. 6, 44 (1966).

[14]M. J. Crooks, Ph. D. thesis, Yale University, 1962 (unpublished).

[15]B. Bertman, H. A. Fairbank, R. A. Guyer, and C. W. White, Phys. Rev. 142, 79 (1966).

[16]J. E. Vos, R. Veenenga Kingma, F. J. Van Gaag, and B. S. Blaisse, Phys. Letters 24A, 738 (1967); O. W. Heybey and C. M. Lee, ibid. 19, 106 (1967).

[17]L. H. Nosanow and N. R. Werthamer, Phys. Rev. Letters 15, 618, 997 (1965).

[18]C. C. Ackerman and R. A. Guyer, Solid State Commun. 5, 671 (1967).

[19]C. Herring, Phys. Rev. 95, 954 (1954).

[20]Peter Meier (private communication).

[21]J. Callaway, Phys. Rev. 162, 731 (1961).

[22]R. Berman, C. Bounds, and J. Rogers, Proc. Roy. Soc. (London) A289, 66 (1965).

[23]R. Berman, C. L. Bounds, C. R. Day, and H. H. Sample, Phys. Letters 26A, 185 (1968).

[24]B. Agrawal, Phys. Rev. 162, 731 (1967).

[25]P. G. Klemens and A. A. Maradudin, Phys. Rev. 123, 804 (1961).

[26]P. G. Klemens, R. De Bruyn Ouboter, and C. Le Pair, Physica 30, 1863 (1964).

[27]Guyer and Sarkissian have applied Eq. (30) to the LiF data of P. D. Thacher, Phys. Rev. 156, 975 (1967), and have obtained results in good agreement with the analysis of Berman and Brock of their LiF data; R. Berman and J. C. F. Brock, Proc. Roy. Soc. (London) A289, 46 (1965). Thus Eq. (30), a computationally simplified version of the Callaway equation, has been used in our analysis.

Transport Coefficients of a Normal Fermi Liquid: Application to Liquid He³ †

K. S. Dy and C. J. Pethick*
Department of Physics, University of Illinois, Urbana, Illinois 61801
(Received 24 April 1969)

The transport coefficients of a normal Fermi liquid in the extreme low-temperature limit and the leading finite-temperature contributions to the transport coefficients are studied using the quasiparticle transport equation. The scattering amplitude for quasiparticles on the Fermi surface is expressed in terms of Landau parameters, using an approximation which takes into account s- and p-wave scattering; the calculated values of the transport coefficients in the extreme low-temperature limit for liquid He³ are shown to be in good agreement with the experimental values. Finite-temperature contributions to the transport coefficients are expressed in terms of the solution of the transport equation in the extreme low-temperature limit, and explicit calculations are performed for the case of liquid He³. Assuming Landau parameters with $l \geq 2$ vanish, an estimate of the Landau parameter F_1^a for liquid He³ is obtained by comparing the theoretical and experimental values of the leading finite-temperature contributions to the transport coefficients.

I. INTRODUCTION

Recent experimental work on the transport properties of liquid He³ and dilute mixtures of He³ in He⁴ has led to renewed interest in the problem of solving the quasiparticle transport equation and of determining the quasiparticle scattering amplitude. Historically, the first method of solving the transport equation was that of Abrikosov and Khalatnikov,[1] who calculated the limiting low-temperature behavior of the coefficient of thermal conductivity K and the coefficient of viscosity η.